Electronic Supplementary Material (ESI) for ChemComm.

Electronic Supplementary Information

Inflating Face-Capped Pd_6L_8 Coordination Cages

Suzanne M. Jansze, Daniel Ortiz, Farzaneh Fadaei Tirani, Rosario Scopelliti, Laure Menin and Kay Severin*

Institut des Sciences et Ingénierie Chimiques, Ecole Polytechnique Fédérale de Lausanne (EPFL), 1015 Lausanne, Switzerland

Table of Contents

1. General

All chemicals were obtained from commercial sources (see below) and used without further purification unless stated otherwise. Solvents were dried using a solvent purification system from Innovative Technologies, Inc.. Reactions were carried out under an atmosphere of dry N_2 using standard Schlenk techniques.

NMR spectra were obtained on a Bruker DRX (^{1}H: 400 MHz, ^{13}C: 101MHz) equipped with a BBO 5 mm probe, a Bruker Avance III spectrometer (^{1}H: 600 MHz, ^{13}C: 151 MHz) equipped with a 5 mm CPTCIz cryo-probe and a Bruker Avance III spectrometer (^{1}H: 400 MHz) equipped with a 5 mm BBFO-Plus probe.

The chemical shifts are reported in parts per million δ (ppm) referenced to the residual solvent signal, unless stated otherwise. All spectra were recorded at 298 K, unless stated otherwise. The analysis of NMR spectra was performed with MestreNova, and for the DOSY analysis the Peak Height Fit DOSY transform from MestreNova was used.

Routine ESI-MS data were acquired on a Q-TOF Ultima mass spectrometer (Waters) operated in the positive ionization mode and fitted with a standard Z-spray ion source equipped with the Lock-Spray interface. Data were processed using the MassLynx 4.1 software.

Commercial sources:

Anhydrous iron(II) chloride – Acros
Nioxime – ABCR
Bis(triphenylphosphine)palladium(II) dichloride – Sigma Aldrich
1,3,5-Tribromobenzene – Apollo Scientific
1,3,5-Tris(4-bromophenyl)benzene – TCI
Bis(pinacolato)diboron – FluoroChem
Sodium (meta)periodate – Sigma Aldrich
Pyridine-3-boronic acid – FluoroChem
Tetrakis(acetonitrile)palladium(II) tetrafluoroborate – ABCR

2. Experimental procedures and characterisation

2.1. Synthesis of triboronic acids C and F

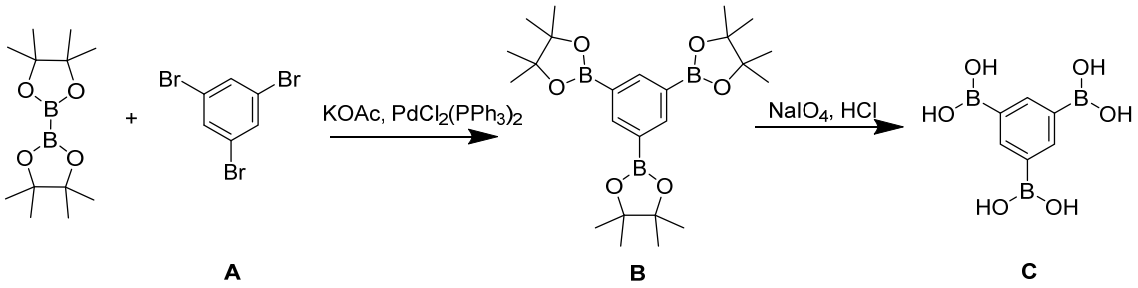

Scheme S1. Synthesis of triboronic acid **C**.

1,3,5-Tribromobenzene **A** (10.0 g, 32 mmol), bis(pinacolato)diboron (26.6 g, 105 mmol, 3.3 eq.), KOAc (10.3 g, 105 mmol, 3.3 eq.), and $PdCl_2(PPh_3)_2$ (1.3 g, 1.9 mmol, 0.06 eq.) were combined in a round bottom flask. Degassed dioxane (250 mL) was added and the reaction was stirred at 120 °C overnight. The reaction is cooled to r.t., filtered, dried under reduced pressure and purified by silica column chromatography (gradient of 20% to 50% EtOAc in Hexane). The pure fractions were dried under reduced pressure, which yielded a white powder which was verified by ^{1}H NMR to be the triboronate ester **B** (9.8 g, 21.5 mmol, 67%). The latter was used directly for the deprotection reaction described below.

^{1}H NMR (400 MHz, Chloroform-*d*) δ 8.36 (s, 3H), 1.33 (s, 36H).

The deprotection reaction was carried out by a modified method of a published procedure.[S1] The triboronate ester **B** (9.8 g, 21.5 mmol) and sodium (meta)periodate (41.3 g, 194 mmol, 9 eq.) were suspended in a mixture of THF (240 mL) and H_2O (60 mL) and stirred at r.t. overnight. Aqueous HCl (2 M, 5 mL) were added and the reaction mixture was stirred for 24 h. Methanol (600 mL) was added, the mixture was filtered and concentrated under reduced pressure. Aqueous HCl (1M, 300 mL) was added and the mixture was left to stir for 2 h at r.t.. The white solid was collected by filtration and dried by air to yield the triboronic acid **C** (3.8 g, 18.3 mmol, 85%).

Characterization

^{1}H NMR (600 MHz, DMSO-d_6) δ 8.15 (s, 3H), 7.81 (s, 6H).

^{13}C NMR (151 MHz, DMSO-d_6) δ 141.98, 131.61 (weak, C-B).

HRMS (ESI): *m/z* calculated for $C_{11}H_{19}B_3NaO_6^+$, (Cationized with Na and 5 x methoxy adducts, from methanol as solvent) 303.1358, found 303.1368 (3.1 ppm).

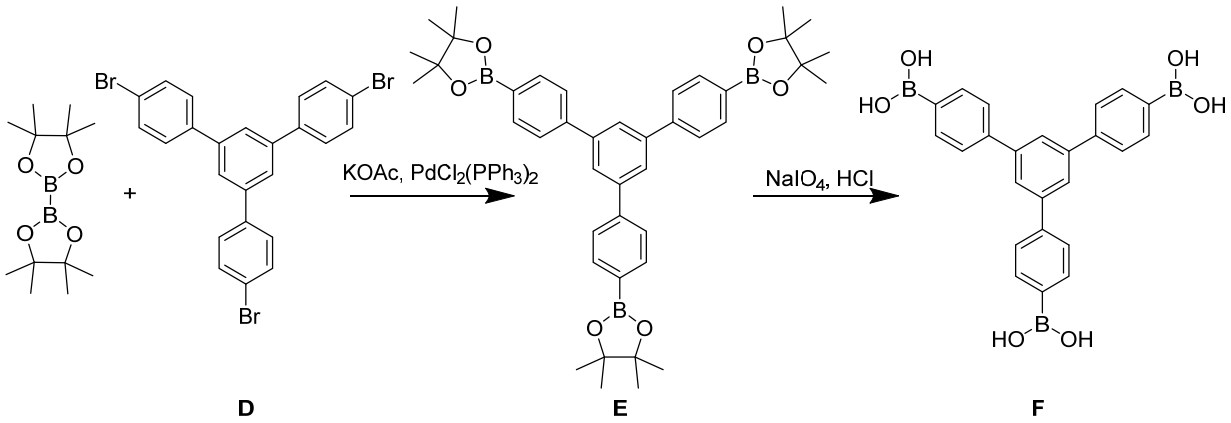

Scheme S1. Synthesis of triboronic acid F.

1,3,5-Tris(4-bromophenyl)benzene **D** (5.0 g, 9.2 mmol), bis(pinacolato)diboron (7.7 g, 30.4 mmol, 3.3 eq.), KOAc (3.0 g, 30.4 mmol, 3.3 eq.), and $PdCl_2(PPh_3)_2$ (0.39 g, 0.18 mmol, 0.06 eq.) were combined in a round bottom flask. Degassed dioxane (100 mL) was added and the reaction was stirred at 120 °C overnight. The reaction was cooled to r.t., filtered, dried under reduced pressure, and purified by silica column chromatography (gradient of 20% to 50% EtOAc in Hexane). The pure fractions were dried under reduced pressure, which yielded a white powder which was verified by ^{1}H NMR to be the triboronate ester **D** (5.3 g, 7.7 mmol, 84%). The latter was used directly for the deprotection reaction described below.

^{1}H NMR (400 MHz, Chloroform-*d*) δ 7.93 (d, *J* = 7.6 Hz, 6H), 7.82 (s, 3H), 7.71 (d, *J* = 7.5 Hz, 6H), 1.38 (s, 36H).

The deprotection reaction was carried out by a modified method of a published procedure.[S1] The triboronate ester **D** (5.3 g, 7.7 mmol) and sodium (meta)periodate (14.7 g, 69 mmol, 9 eq.) were suspended in a mixture of THF (100 mL) and H_2O (25 mL) and stirred at r.t. overnight. Aqueous HCl (2 M, 2 mL) were added and the reaction mixture was stirred for 24 h. Methanol (400 mL) was added, the mixture was filtered and concentrated under reduced pressure. Aqueous HCl (1M, 120 mL) was added and the mixture was left to stir for 2 h at r.t.. The white solid was collected by filtration and dried by air to yield the triboronic acid **F** (3.2 g, 7.3 mmol, 95%).

Characterization

^{1}H NMR (400 MHz, DMSO-d_6) δ 8.11 (s, 6H), 7.93 (d with s overlapping, 9H), 7.85 (d, *J* = 7.7 Hz, 6H).

^{13}C NMR (101 MHz, DMSO-d_6) δ 141.58, 141.50, 134.78, 126.15, (C-B not detected).

HRMS (ESI): *m/z* calculated for $C_{29}H_{30}B_3NaO_{6+}{}^+$, (Cationized with Na and 5 x methoxy adducts, from methanol as solvent) 531.2317, found 531.2313 (0.8 ppm).

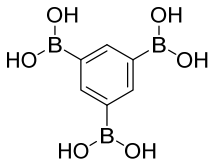

C

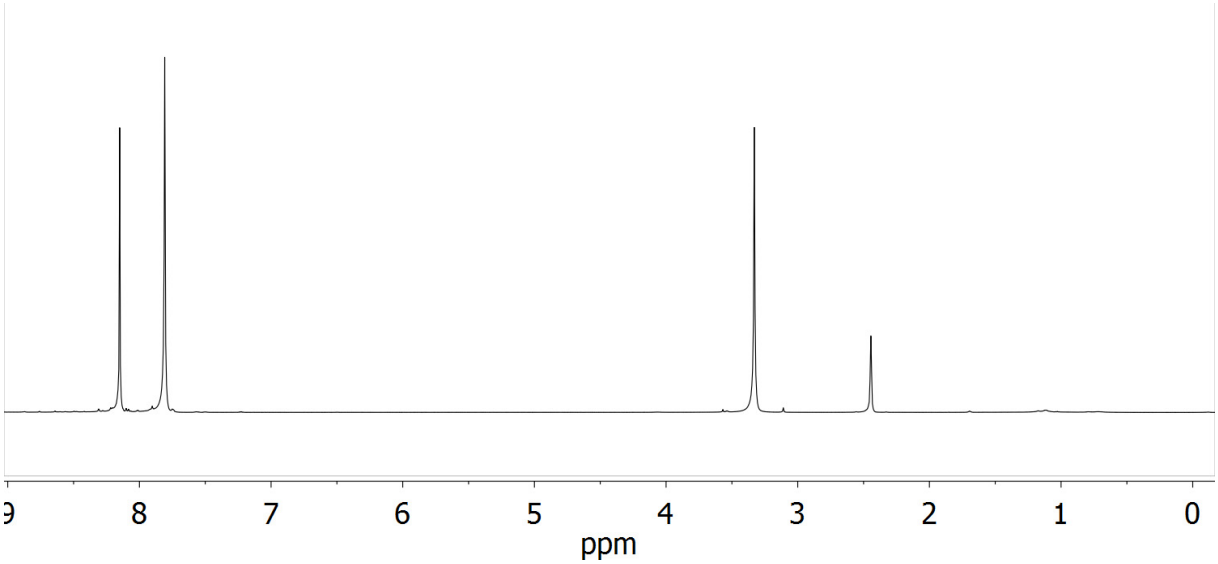

Figure S1. ^{1}H NMR spectrum of triboronic acid **C** in DMSO-d_6.

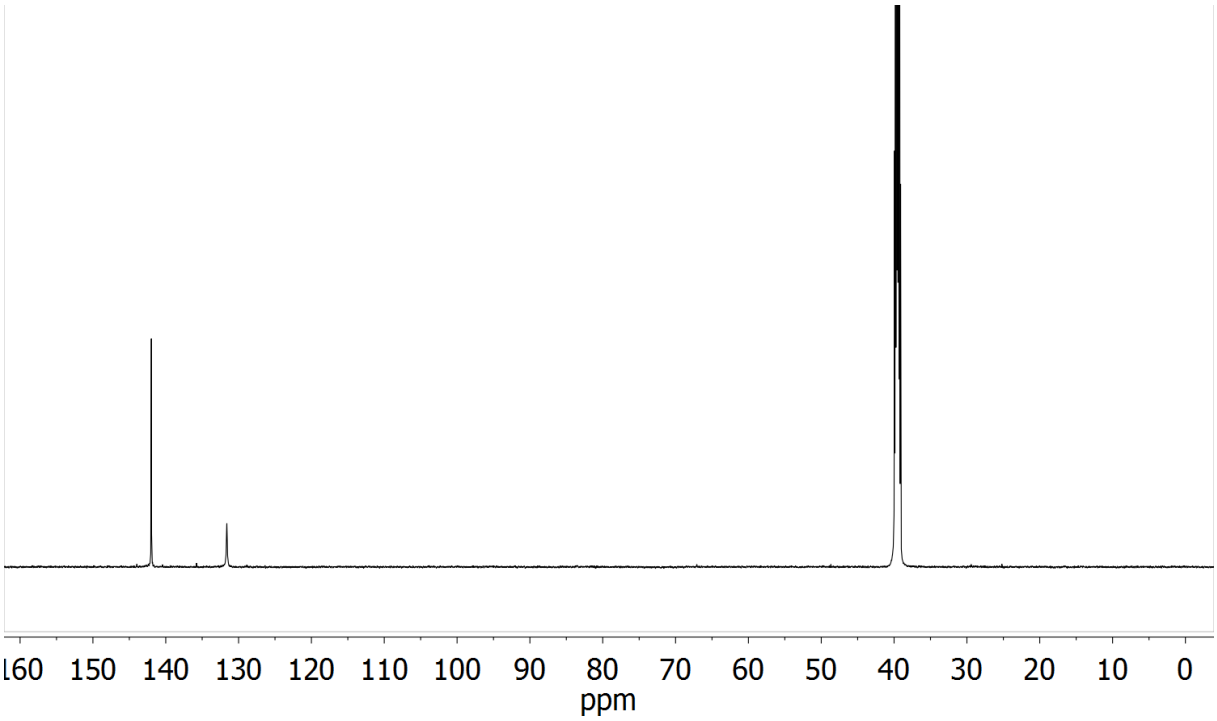

Figure S2. ^{13}C NMR spectrum of triboronic acid **C** in DMSO-d_6.

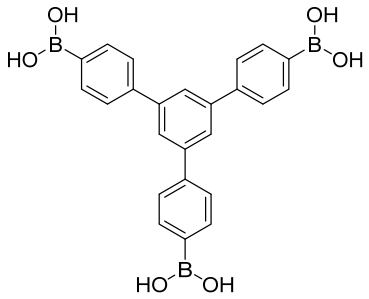

F

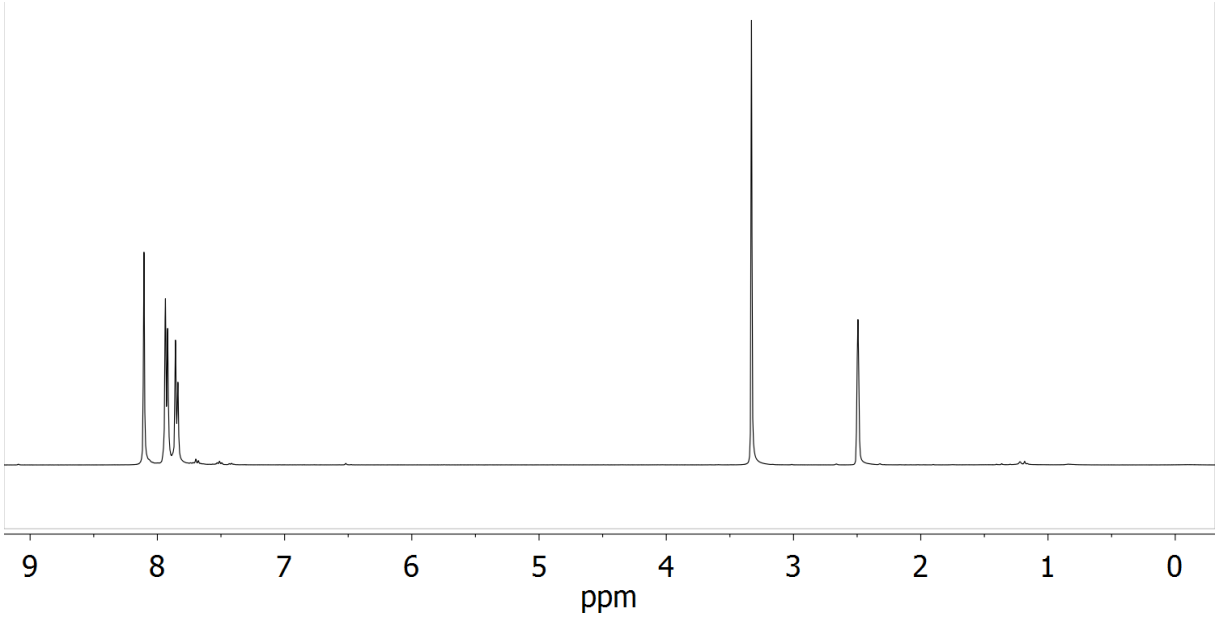

Figure S3. ^{1}H NMR spectrum of triboronic acid **F** in DMSO-d_6.

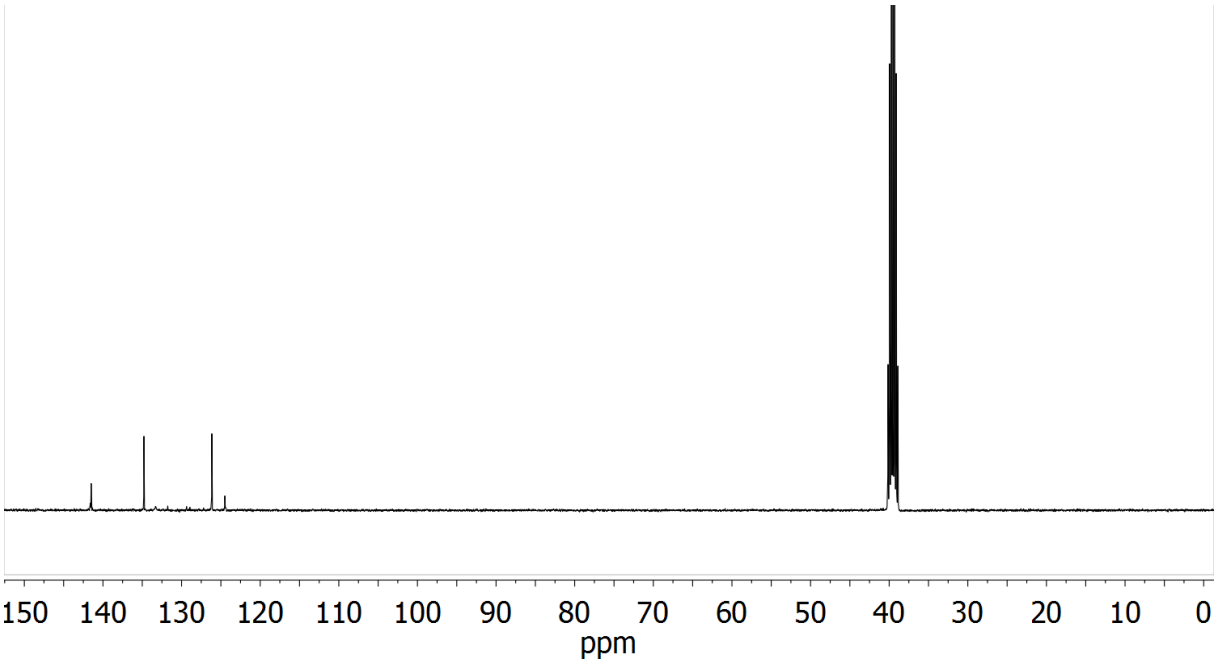

Figure S4. ^{13}C NMR spectrum of triboronic acid **F** in DMSO-d_6.

2.2. Synthetic procedure for clathrochelate ligands L1 and L2

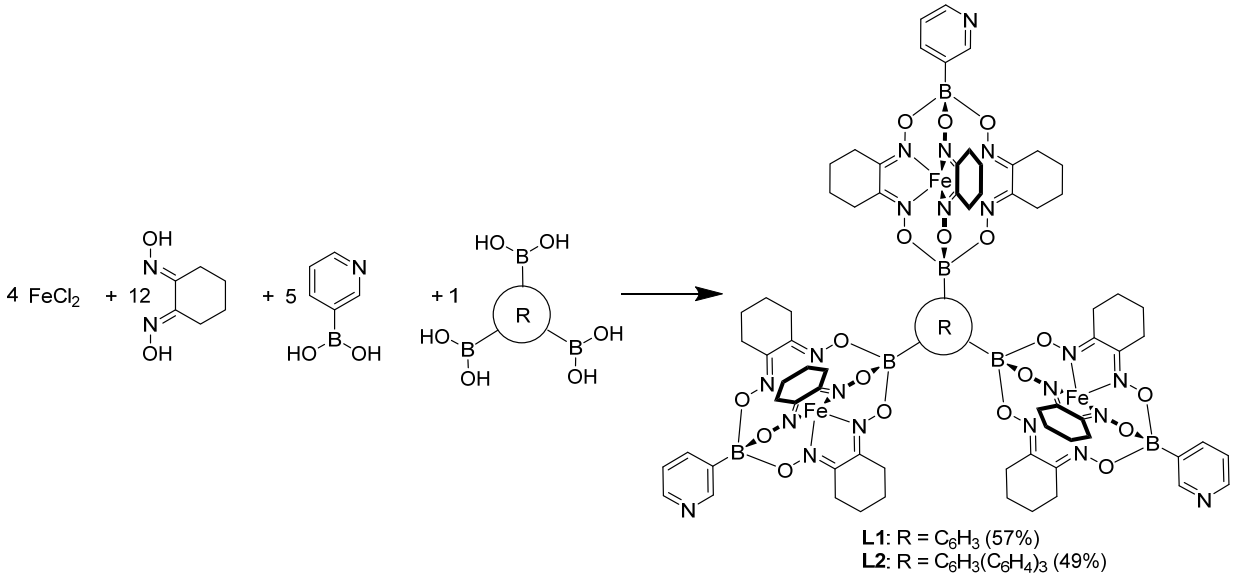

Scheme S3. Synthesis of the metalloligands **L1** and **L2**.

Anhydrous $FeCl_2$ (4 eq.) and the respective dioxime (12 eq.) were dissolved in MeOH (15 mL). In a separate flask, the respective triboronic acid (100 mg, 1 eq.) and 3-pyridine boronic acid (5 eq.) were dissolved in methanol (20 mL), acetone (5 mL), and chloroform (150 mL) and heated to reflux and stirred for 30 min. The pre-prepared mixture of dioxime and $FeCl_2$, was added to the boronic acid mixture, the mixture was heated to reflux for an additional 3 h, before the solvent was removed under reduced pressure. The remaining solid was dissolved in $CHCl_3$ (100 mL), filtered and washed with a saturated aqueous solution of sodium EDTA and 5% ammonia (100 mL). The organic phase was dried over $MgSO_4$, and evaporated under reduced pressure. The solid was pre-purified by a short silica column (150 g silica, 10% MeOH in DCM) to remove any polymeric material. The dark red fractions were evaporated under reduced pressure, the solid was dissolved in DCM (10 mL), filtered over H-PTFE 20/25 syringe filters and separated on a size exclusion column (200 g, dry weight, Bio-Beads S-X3 in DCM). The pure fractions (checked by MS, pos. mode), were combined and washed with saturated $NaHCO_3$ solution, dried over $MgSO_4$, and the solvent was removed under reduced pressure to yield a red powder.

Table S1. Amounts used for the synthesis of the metalloligands **L1** and **L2**. BA is boronic acid, CC is clathrochelate.

Ligand	tri-BA	4 eq. $FeCl_2$		12 eq. nioxime		1 eq. tri-BA		5 eq. 3-pyridine BA		Yield		
#	#	mg	Mmol	mg	mmol	mg	mmol	mg	mmol	mg	mmol	%
L1	**C**	290	2.3	977	6.9	120	0.60	352	2.9	435	0.35	57
L2	**F**	198	1.6	667	4.7	100	0.39	288	2.3	262	0.20	49

Characterization

L1: ^{1}H NMR (400 MHz, DCM-d_2) δ 8.81 (s, 3H), 8.51 (d, J = 3.5 Hz, 3H), 7.99 – 7.84 (m, 6H), 7.29 – 7.16 (m, 3H), 2.95 (2 s, 36H), 1.83 (s, 36H). ^{13}C NMR (151 MHz, DCM-d_2) δ 153.49, 152.61, 152.06, 151.81, 149.42, 139.72, 123.33, 26.79, 26.70, 22.23, 22.19, (C-B not detected). HRMS (ESI): *m/z* calculated for $C_{75}H_{90}B_6Fe_3N_{21}O_{18}$ $[M+3H]^{3+}$ 602.1813, found 602.1818 (0.8 ppm)

L2: ^{1}H NMR (400 MHz, DCM-d_2) δ 8.81 (s, 3H), 8.51 (d, J = 4.8 Hz, 3H), 7.98 – 7.70 (m, 21H), 7.32 – 7.16 (m, 3H), 2.95 (2 s, 36H), 1.84 (s, 36H). ^{13}C NMR (151 MHz, DCM-d_2) δ 153.48, 152.80, 152.61, 149.45, 143.23, 141.12, 139.72, 132.73, 125.32, 123.35, 26.82, 26.77, 22.14, (C-B not detected). HRMS (ESI): *m/z* calculated for $C_{93}H_{102}B_6Fe_3N_{21}O_{18}$ $[M+3H]^{3+}$ is 678.2128, found 678.2145 (2.5 ppm)

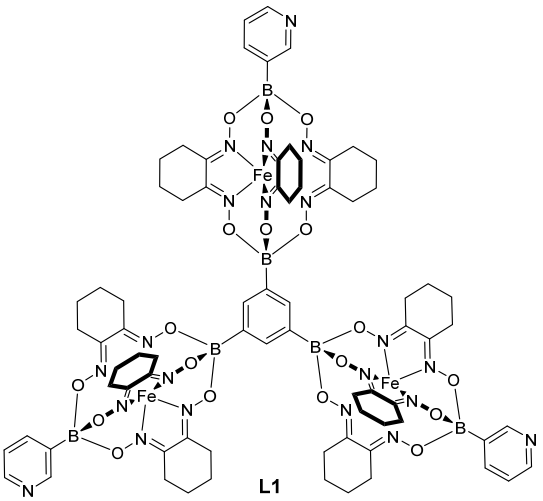

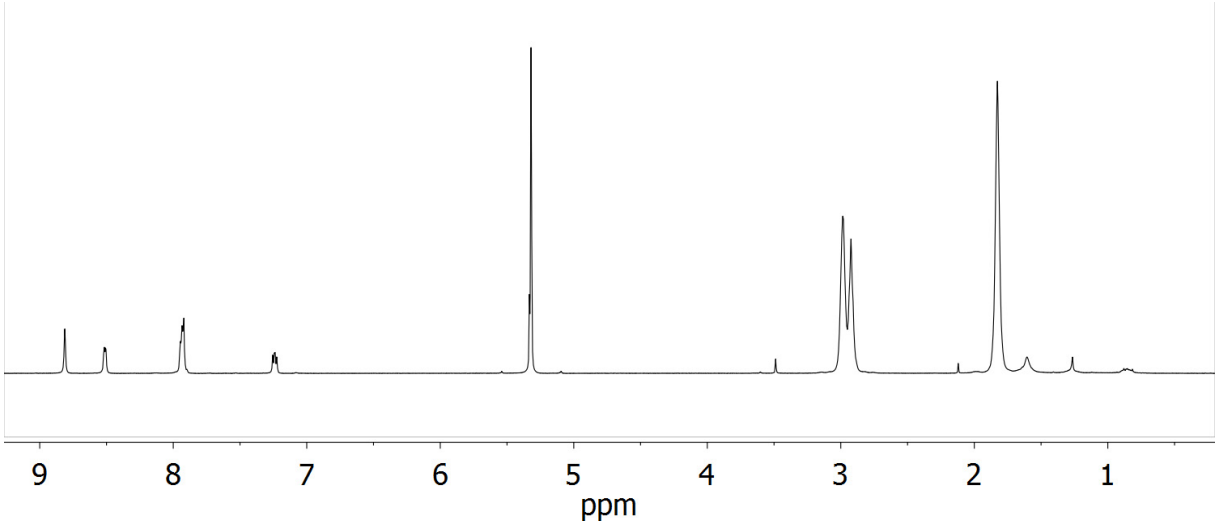

Figure S5. ^{1}H NMR spectrum of **L1** in DCM-d_2.

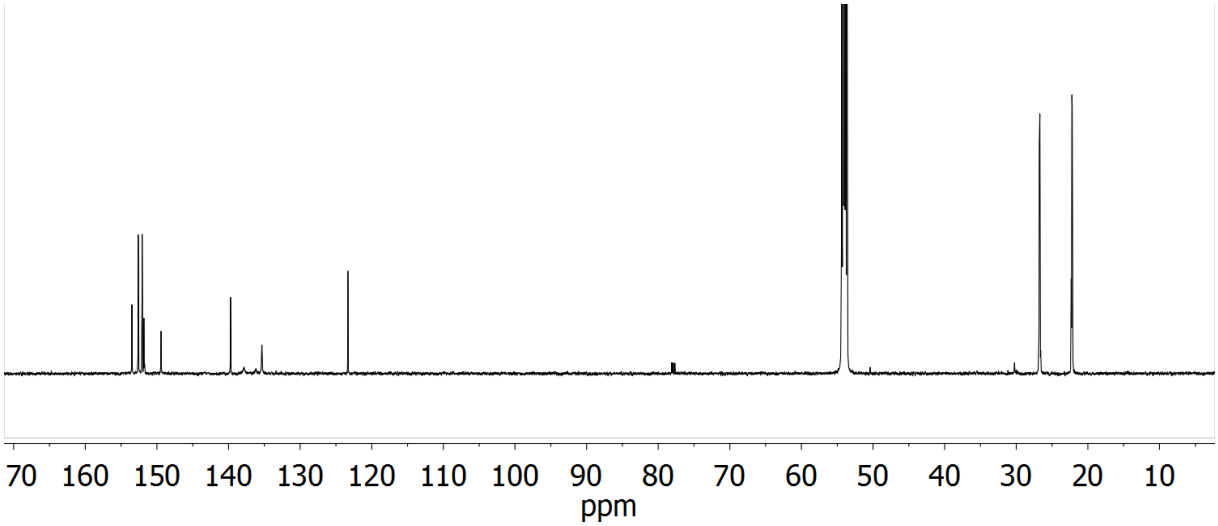

Figure S6. ^{13}C NMR spectrum of **L1** in DCM-d_2.

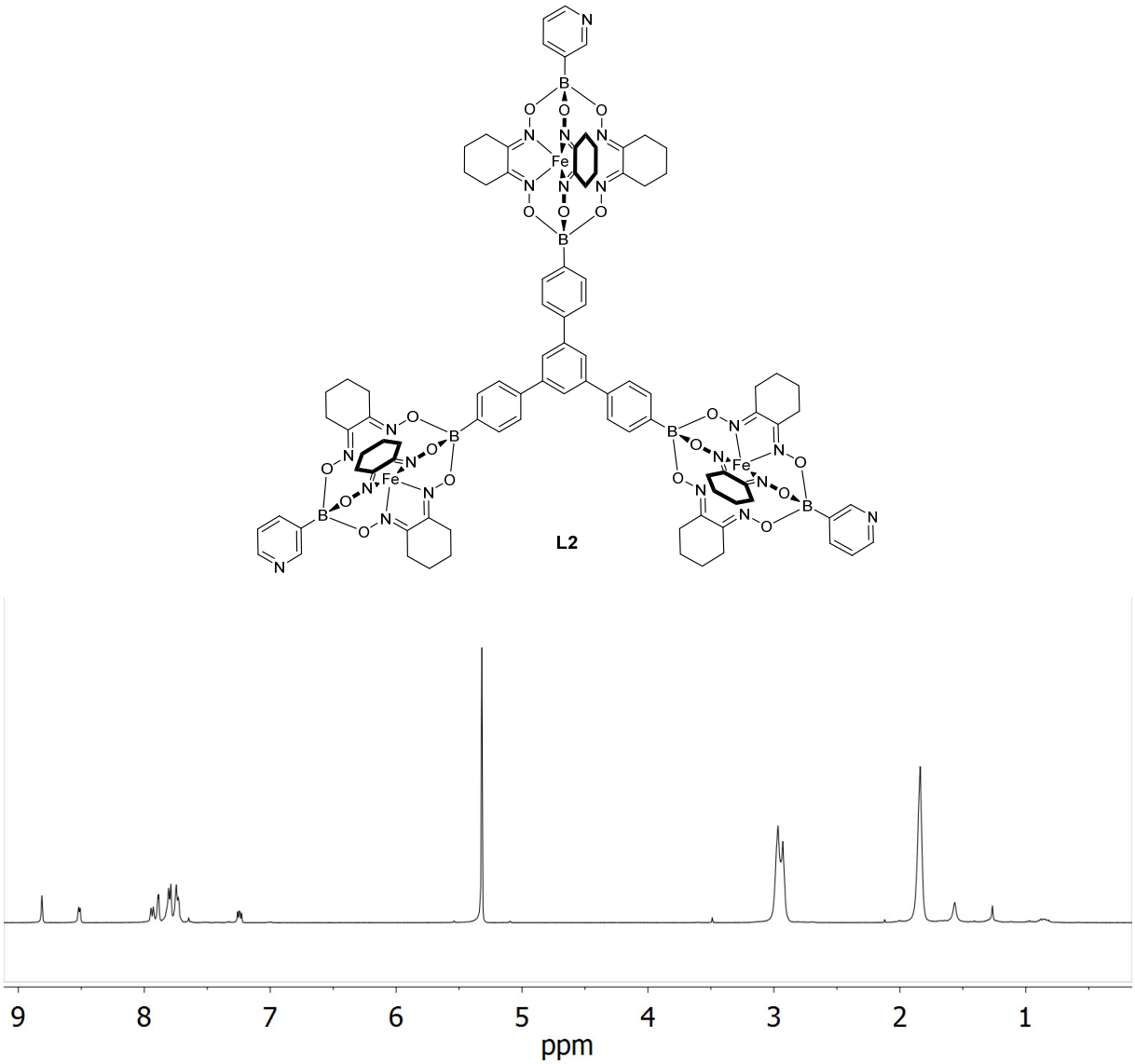

Figure S7. ^{1}H NMR spectrum of **L2** in DCM-d_2.

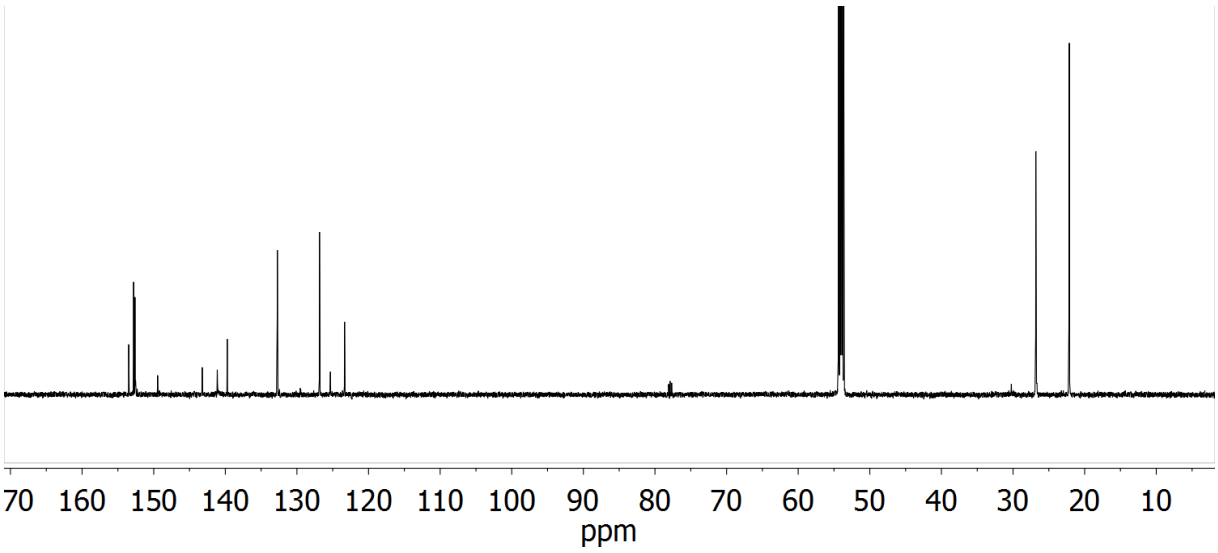

Figure S8. ^{13}C NMR spectrum of **L2** in DCM-d_2.

2.3. General synthesis procedure for Pd_6L_8 coordination cages.

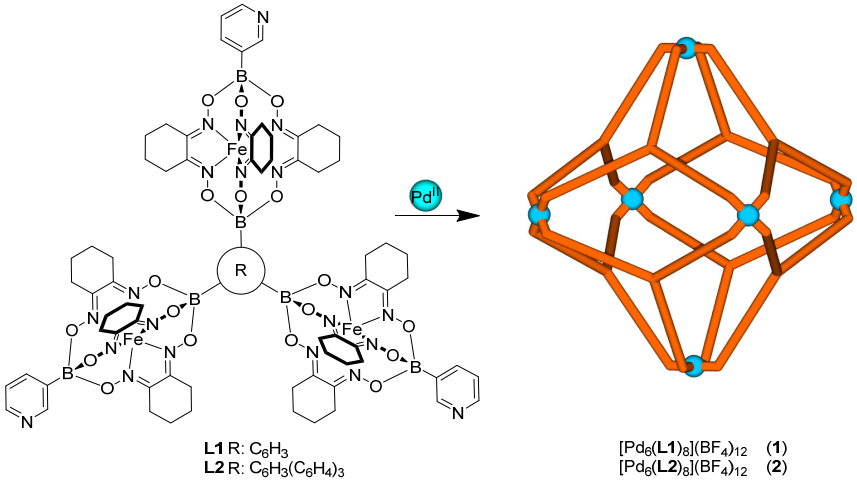

Scheme S4. Synthesis of the Pd_6L_8 coordination cages **1** and **2** from **L1** and **L2**

To the metalloligand (see Table S2 for amounts, 1.5 µmol, 4 eq.) and $[Pd(CH_3CN)_4](BF_4)_2$ (0.5 mg, 1.1 µmol, 3 eq.) 0.6 mL of DMSO-d_6 was added. The solution was heated at 70 °C for 17 h, in which the solution went from turbid to a clear red solution with everything dissolved. NMR shows full conversion to yield the Pd_6L_8 coordination cages.

Table S2. The amounts of the double clathrochelates used for the synthesis of the M_2L_4 coordination cages.

Metalloligand #	**Amount used (mg)**
L1	2.7
L2	3.0

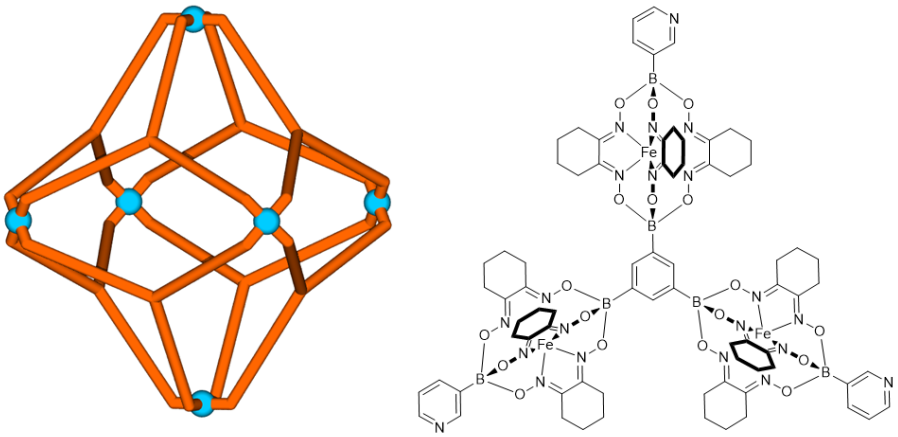

M_6L_8 cage (**1**) from ligand **L1**

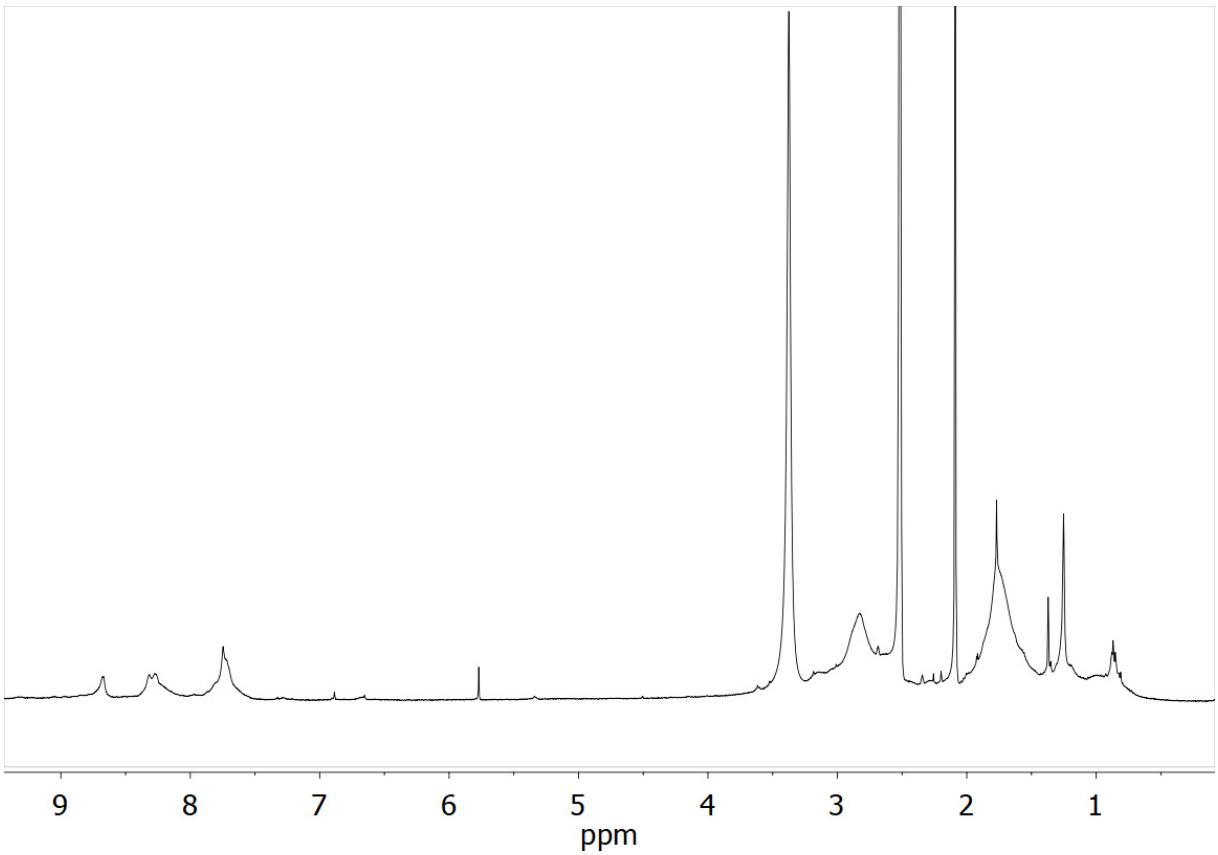

Figure S9. ^{1}H NMR spectrum of complex **1** in DMSO-d_6. Despite extensive attempts to dry the ligand, there is still a minor solvent peak of the DCM visible.

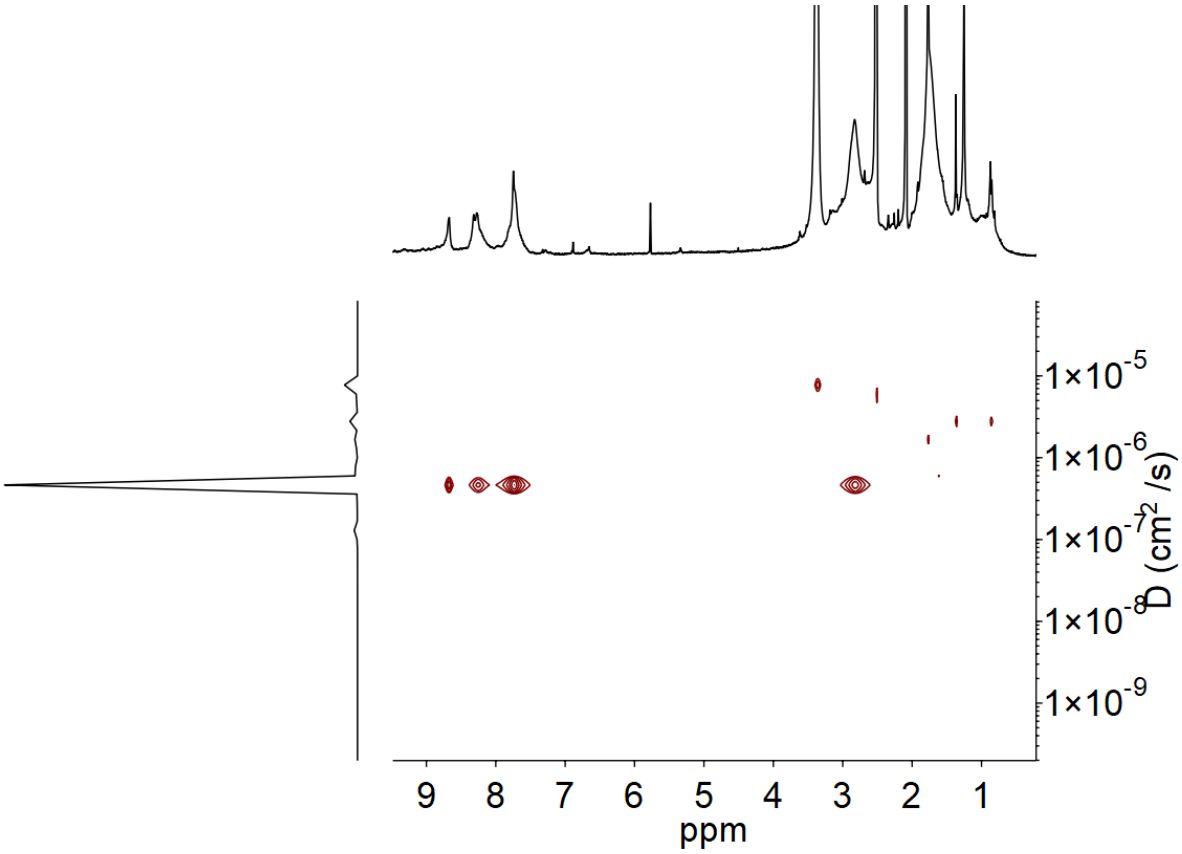

Figure S10. ^{1}H DOSY NMR spectrum of complex **1** in DMSO-d_6. Despite extensive attempts to dry the ligand, there is still a minor solvent peak of the DCM visible. The DOSY transform from MestreNova also seems to be unable to find both the broad (and overlapping peaks) that belong to the cyclohexyl groups of the triple clathrochelate.

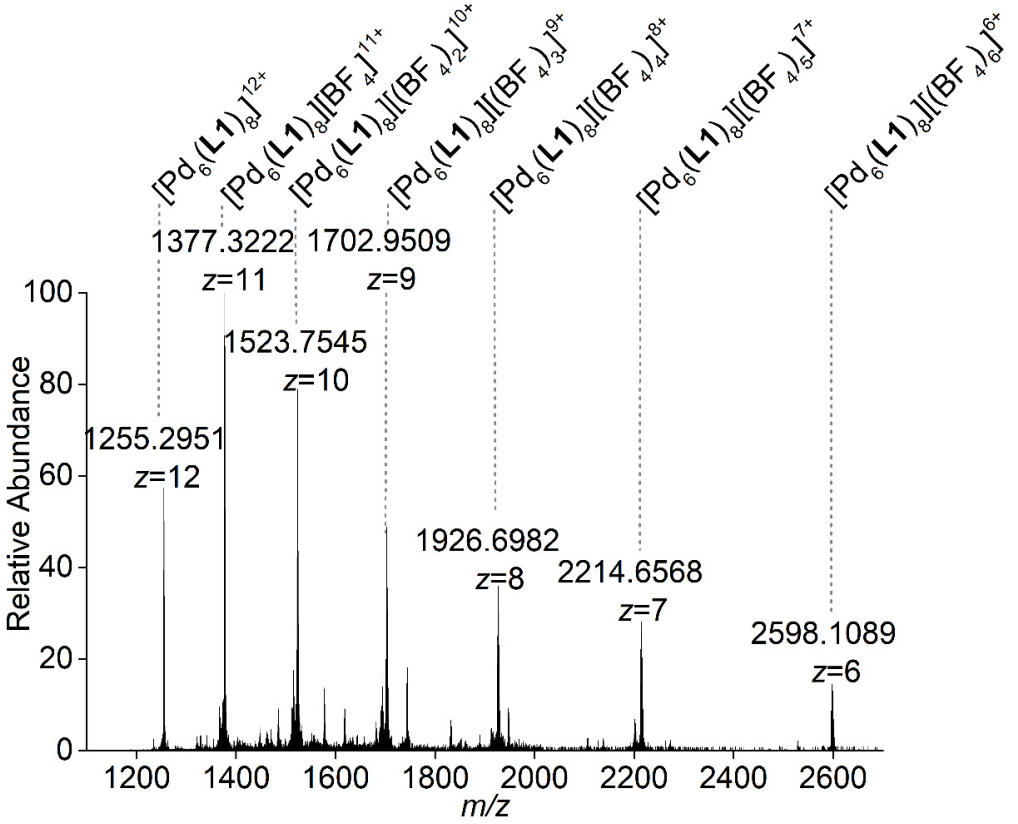

Figure S11. HRMS Cold-Spray Ionisation spectrum of coordination cage **1** in DMSO / CH_3CN (10:90).

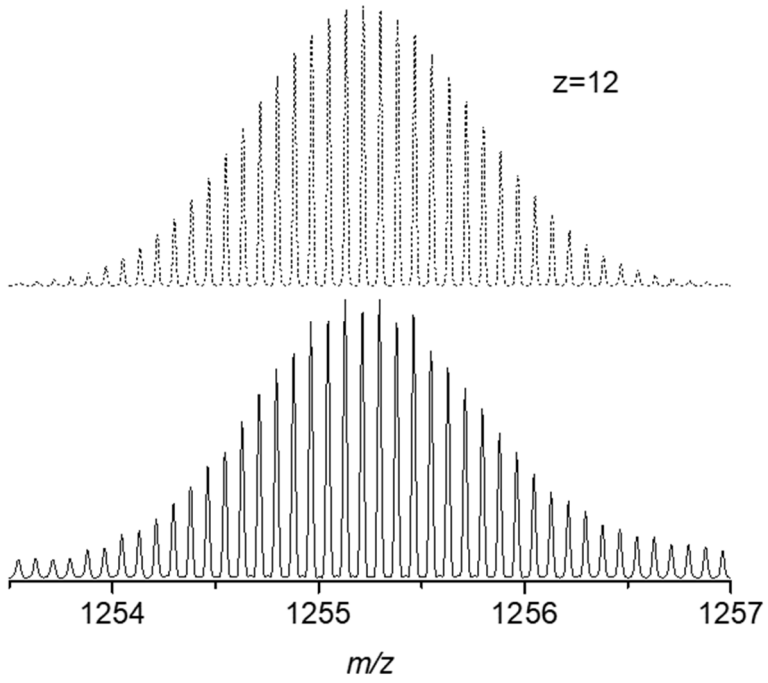

Figure S12. HRMS Cold-Spray Ionisation mass spectrum of coordination cage **1** in DMSO / CH_3CN (10:90). Zoom-in around the 1255 *m/z* region (bottom). Simulated mass spectrum of the +12 charge species of the complex $[Pd_6(L1)_8]^{12+}$ (top).

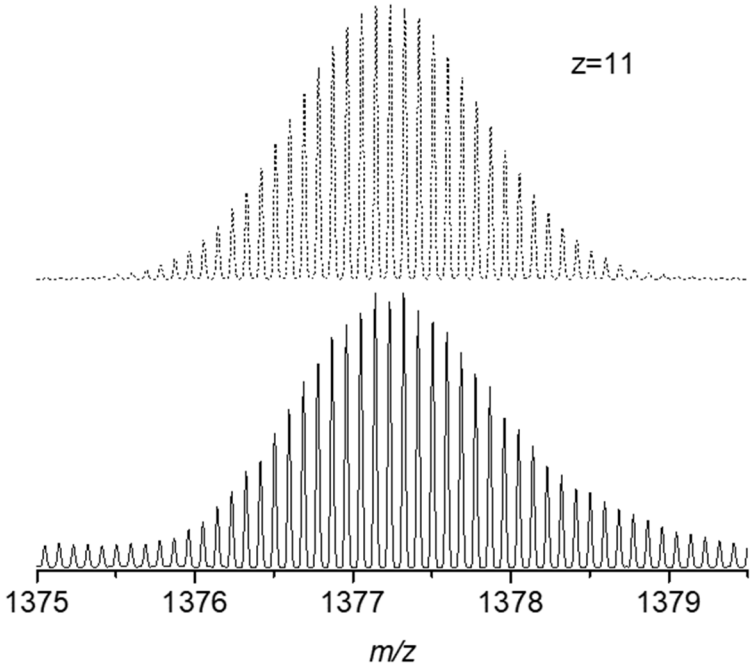

Figure S13. HRMS Cold-Spray Ionisation mass spectrum of coordination cage **1** in DMSO / CH_3CN (10:90). Zoom-in around the 1377 *m/z* region (bottom). Simulated mass spectrum of the +11 charge species of the complex $[Pd_6(L1)_8][BF4]^{11+}$ (top).

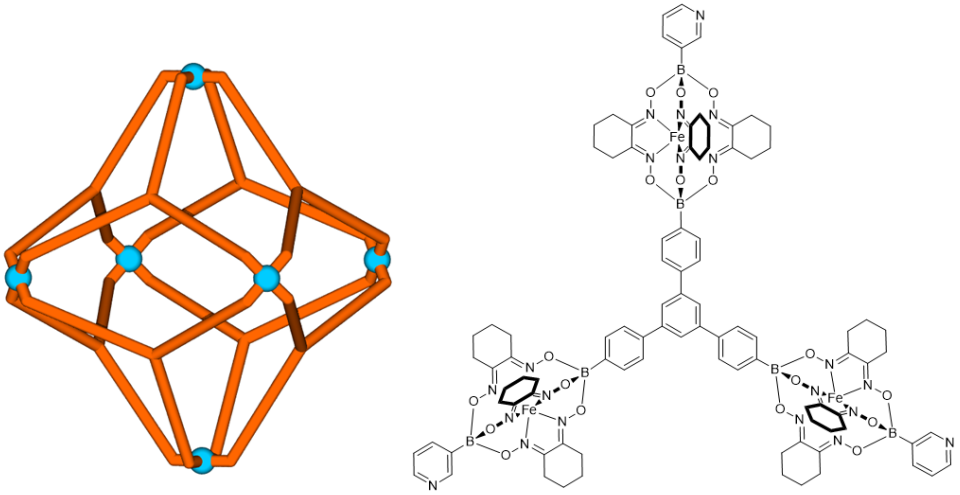

M_6L_8 cage (**2**) from ligand **L2**

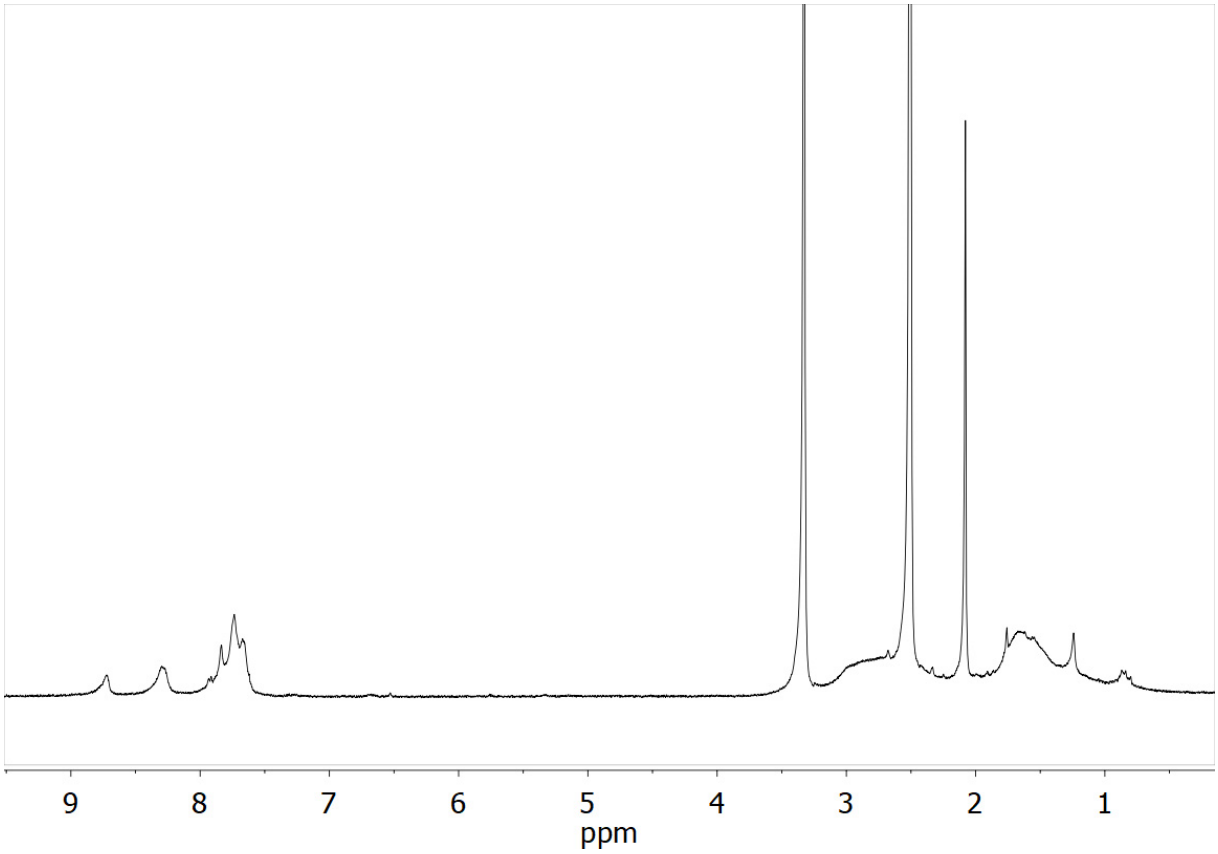

Figure S14. ^{1}H NMR spectrum of complex **2** in DMSO-d_6.

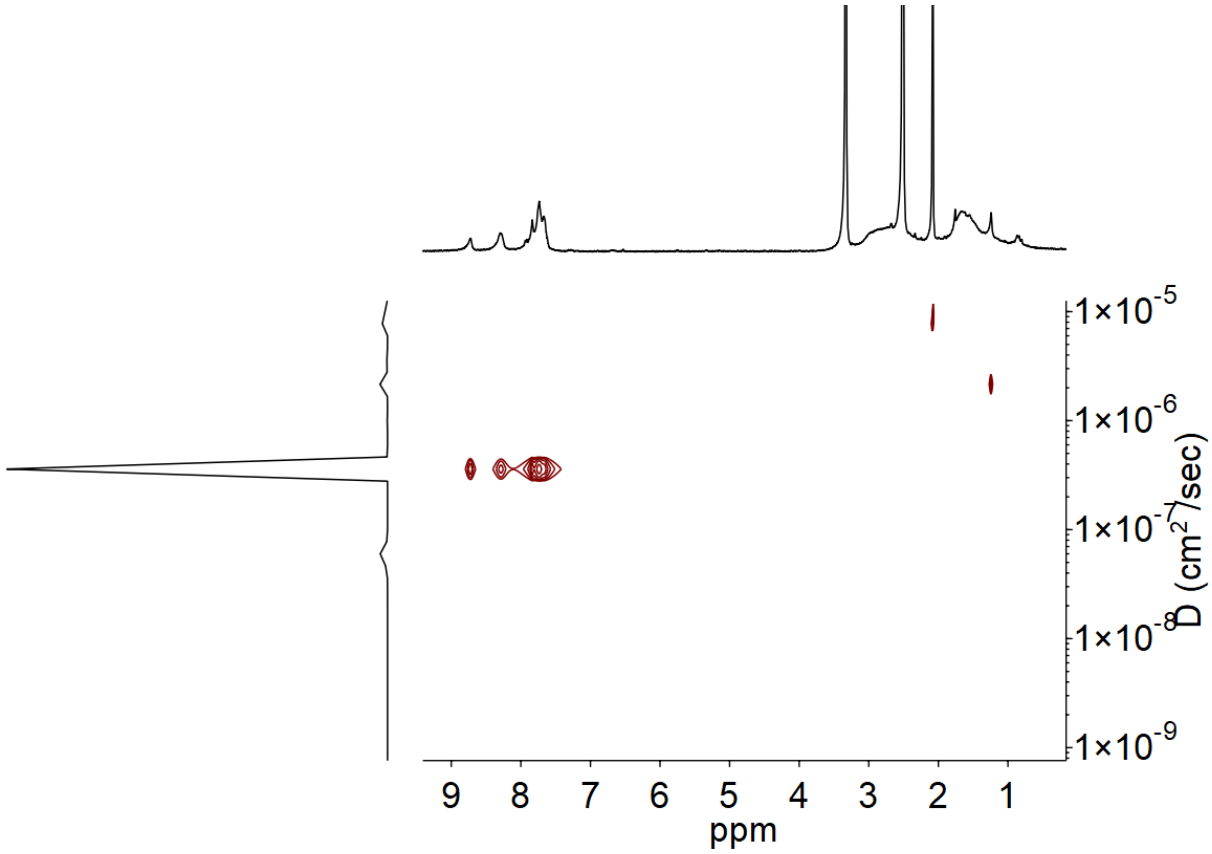

Figure S15. ^{1}H DOSY NMR spectrum of complex **2** in DMSO-d_6. The DOSY transform from MestreNova also seems to be unable to find both the broad (and overlapping peaks) that belong to the cyclohexyl groups of the triple clathrochelate.

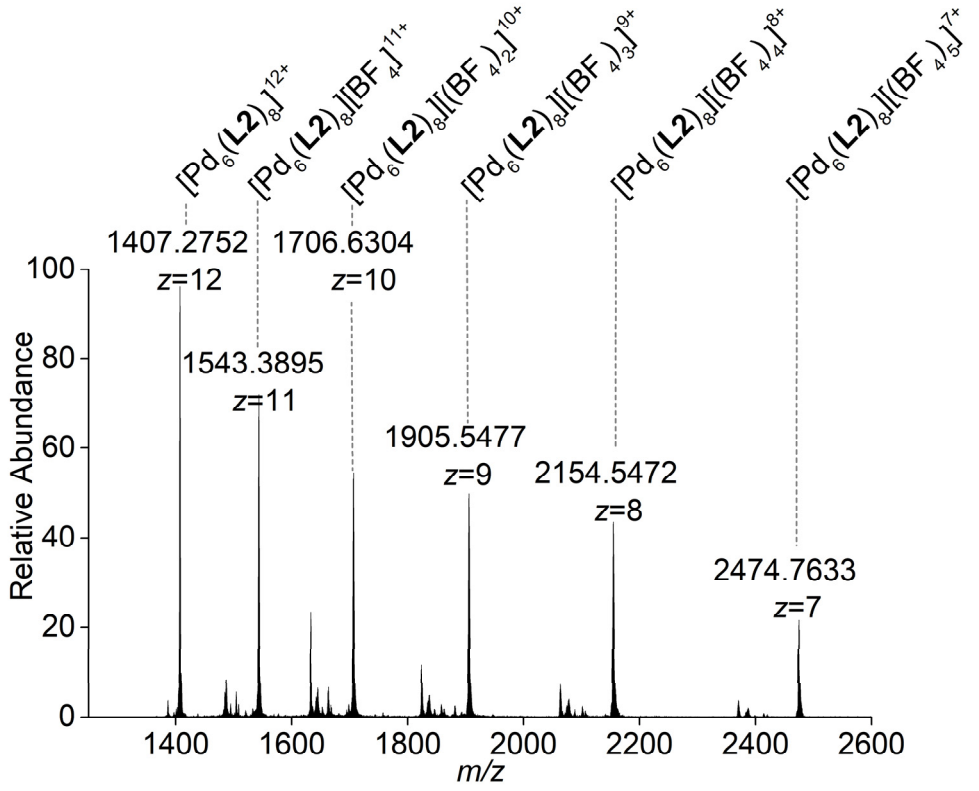

Figure S16. HRMS Cold-Spray Ionisation mass spectrum of coordination cage **2** in DMSO / CH_3CN (10:90).

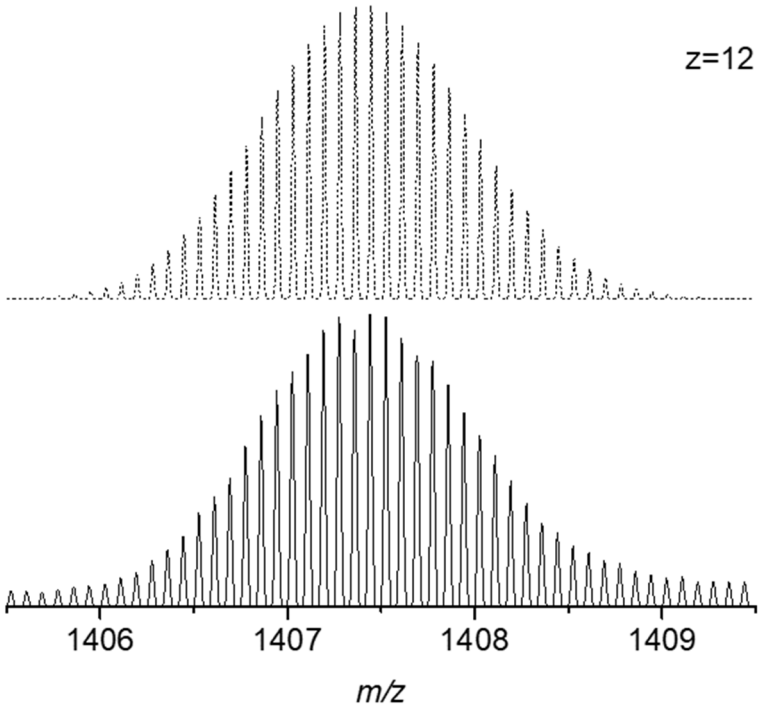

Figure S17. HRMS Cold-Spray Ionisation mass spectrum of coordination cage **2** in DMSO / CH_3CN (10:90). Zoom-in around the 1407 *m/z* region (bottom). Simulated mass spectrum of the +12 charge species of the complex $[Pd_6(L2)_8]^{12+}$(top).

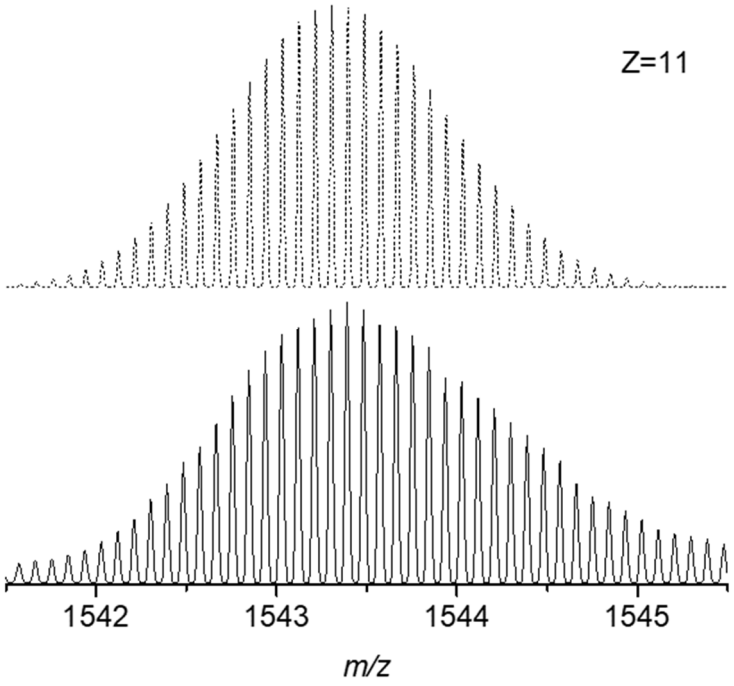

Figure S18. HRMS Cold-Spray Ionisation mass spectrum of coordination cage **2** in DMSO / CH_3CN (10:90). Zoom-in around the 1543 *m/z* region (bottom). Simulated mass spectrum of the +11 charge species of the complex $[Pd_6(L2)_8][BF_4]^{11+}$ (top).

Table S3. HRMS summary of coordination cages 1 ($[Pd_6(L1)_8]^{12+}$ and $[Pd_6(L1)_8][BF4]^{11+}$) and 2 ($[Pd_6(L2)_8]^{12+}$ and $[Pd_6(L2)_8][BF_4]^{11+}$) in DMSO / CH_3CN (10:90). Values correspond to the monoisotopic mass**.**

Metalloligand #	Elemental composition	Mass (Da)	Theoretical (charge)	Experimental	Error (ppm)
L1	$C_{600}H_{696}B_{60}Fe_{24}N_{168}O_{144}Pd_6F_{48}$	16107.57	1255.2941 (+12)	1255.2951	0.7
			1377.3212 (+11)	1377.3223	0.7
L2	$C_{744}H_{792}B_{60}Fe_{24}N_{168}O_{144}Pd_6F_{48}$	17932.32	1407.3567 (+12)	1407.3590	1.6
			1543.2076 (+11)	1543.2092	1.1

3. Cold-Spray ionisation MS

Cold-spray ionisation (CSI) MS was performed on a hybrid linear ion trap (LTQ) Orbitrap Elite mass spectrometer (Thermo Scientific, Bremen, Germany) equipped with a modified HESI-II probe in an Ion Max ion source. In order to perform CSI-MS experiments, the commercial sheath (blue in Figure S19) and auxiliary (green in Figure S19) gas lines were modified and redirected towards a liquid nitrogen cooling device (black in Figure S19).

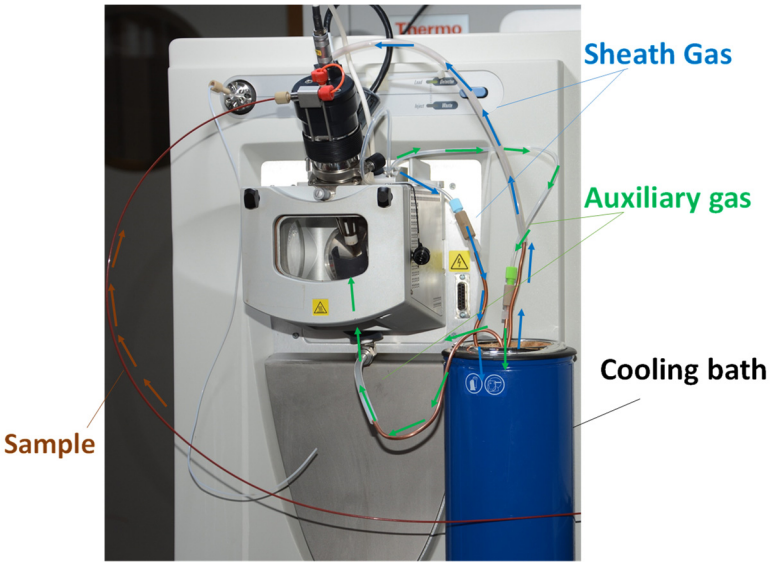

Figure S19. Modified HESI-II probe in an Ion Max ion Source (Thermo Scientific). The sheath gas pathway is represented in blue whereas the auxiliary gas line is in green. Both lines are modified and redirected through the cooling bath.

In the probe body, the sheath gas (inner coaxial N_2) emerging from the metal needle sprays the sample after being redirected through the cooling bath. The auxiliary gas is redirected to the same cooling bath before entering a homemade PVC chamber located at the bottom of the source and helping in stabilizing the temperature as well as the spray (Figure S20).

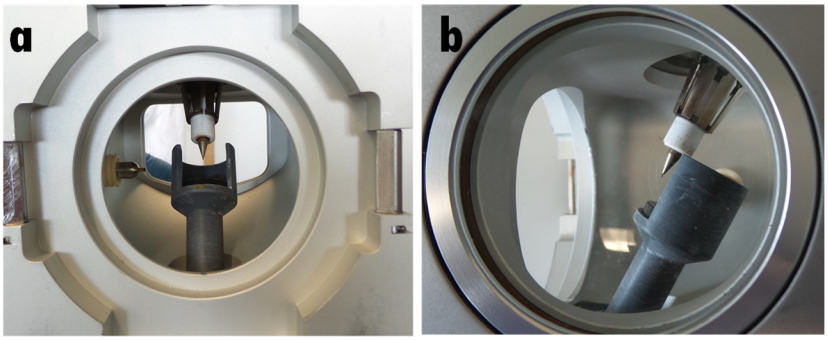

Figure S20. a) Left side and b) Front/back view of the HESI-II probe with the homemade PVC piece placed at the bottom of the Ion Max ion source.

The PVC piece used to redirect the auxiliary gas is composed of three different parts. The main PVC body (Figure S21a) drives the cooled gas towards the entrance of the Orbitrap. A perforated disk (Figure S21b) diffuses the auxiliary gas and is crucial to give a stable signal. Both pieces are attached to the HESI-II probe using a third PVC clamp (Figure S21c).

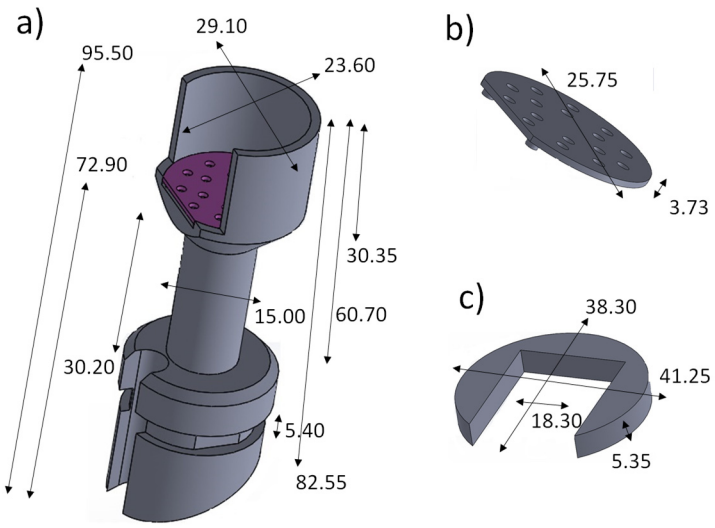

Figure S21. Measurements and design of the homemade PVC pieces contained in the CSI source; a) main body, b) gas diffuser and c) attachment piece. Values are in mm.

The spray temperature is dependent on the cooling bath composition and therefore temperature, the length of the tubing (inside and outside the bath), the materials chosen for the lines as well as the gas flow rates. Therefore, calibration curves were made by placing a thermocouple near the spray, in order to know the instant spray temperature under different conditions of gas flow rates. The liquid nitrogen was used as refrigerant in the cooling bath, the spray temperature was manually controlled by adjusting both the sheath and the auxiliary gas flows, allowing a range of temperature from 20 °C to –50 °C (Figure S22). For this particular setup applied to the mass spectrum measurement of coordination cages, the sheath and auxiliary gas flows were fixed at 6 and 4, respectively, to obtain a spray temperature around –10 °C. This temperature was shown to be the best to both preserve the integrity of coordination cages and obtain sufficient number of ions in the gas phase.

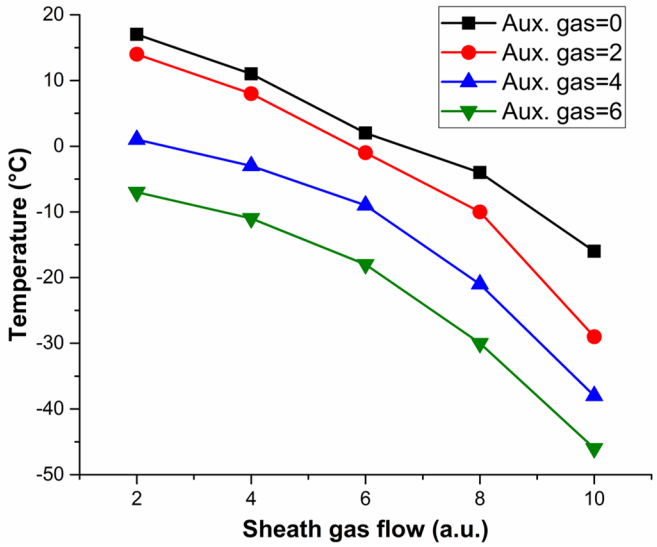

Figure S22. Measured spray temperatures depending on both sheath and the auxiliary gas flows.

High resolution mass spectra were acquired for pure, pre-synthesized samples of the cages. The analytes were diluted in acetonitrile to a final concentration of ~10-20 µM. The standard XCalibur 2.2 data acquisition and instrument control system was utilized (Thermo Scientific). Samples were introduced at a flow rate of 20 µL/min and sprayed using an ionization voltage of +1.2 kV and an ion transfer capillary

temperature of 80 °C. FT-MS spectra were acquired using the high mass range (between 400–4000 *m/z*) in the reduced profile mode with a resolution set to 120'000 at 400 *m/z* and a target value of charges of 1 million. All Orbitrap FTMS scans were recorded averaging 10 microscans to improve the SNR and setting a maximum injection time value at 1000 ms.

4. CCDC data analysis

For the database search, the program ConQuest was used with a CCDC database updated on Feb 2018.

The query that was searched:

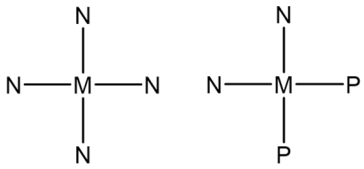

M= Pd or Pt

With the following additional requirements for the molecular formula: M>1, N>3 and C>40

The indication “Size” is the max M-M distance.

Cage **1** (maximum Pd···Pd distance of 3.3 nm) was included for the construction of the graph in red.

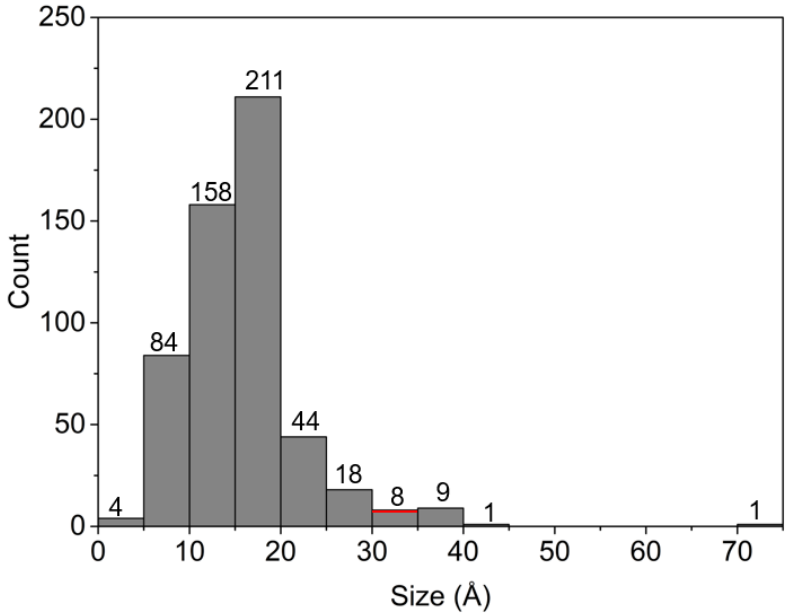

Figure S23. Graphical representation of a CCDC analysis of supramolecular complexes containing Pd. For the construction of this graph, all complexes with Pd atoms from the search were included. The data for cage **1** is included in red.

The database analysis reveals that the majority of the structures have maximum Pd···Pd distances below 2 nm, and only few assemblies have a ‘Size’ of more than 3 nm. Complex **1** is among those assemblies.

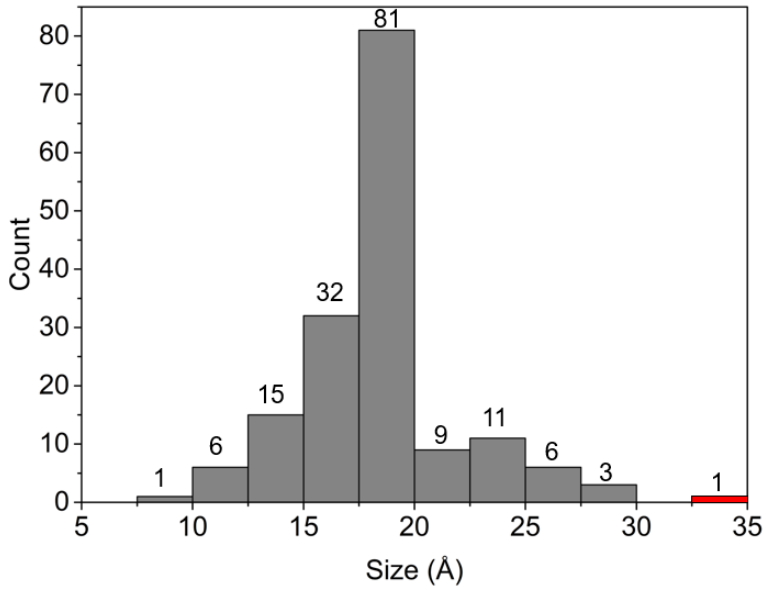

Figure S24. Graphical representation of a CCDC analysis of supramolecular complexes with 6 Pd or Pt ions. For the construction of this graph all complexes with 6 Pd or Pt from the search were included. The data for cage **1** is included in red.

5. VOIDOO calculations cage 1

In order to determine the available void space (probe-occupied volume) within complex **1**, VOIDOO calculations[S2] based on the crystal structure were performed. A virtual probe with a radius of 3.0 Å (smallest probe-size where the probe didn't fall out of the cavity) was employed, and the standard parameters were used, unless noted below.

Maximum number of volume-refinement cycles: 30

Minimum size of secondary grid: 3

Grid for plot files: 0.3

Primary grid spacing: 0.1

Plot grid spacing: 0.1

For complex **1**, the following values were found: Volume: 2.79 x 10^3 Å^3 (standard deviation 0.87 Å^3), which would correspond to a sphere with a radius of 8.74 Å.

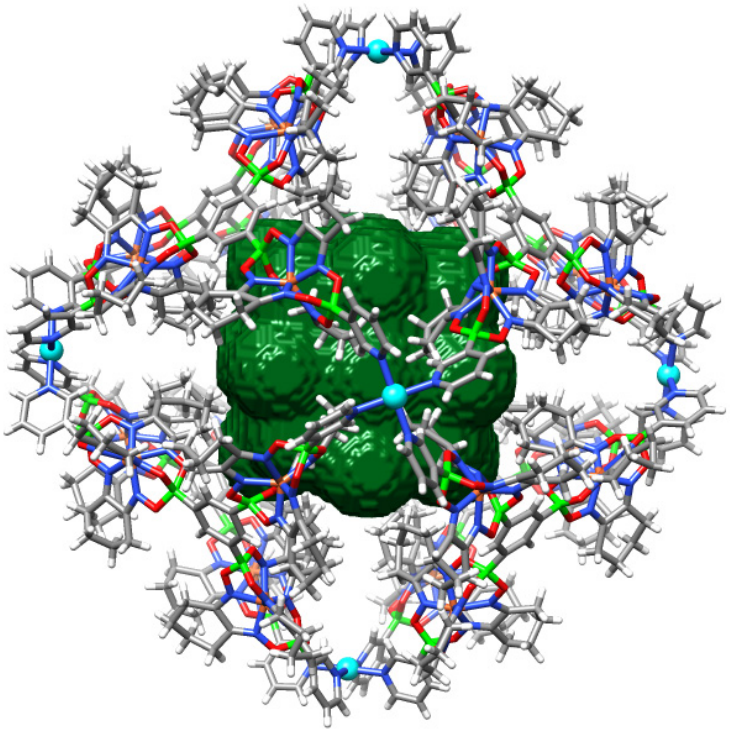

Figure S25. Graphical representation of the main calculated void (dark green) in cage **1**, as calculated with VOIDOO.

6. Spartan model cage 2

A model of cage **2** was constructed using Spartan and it's MMF energy minimisation.

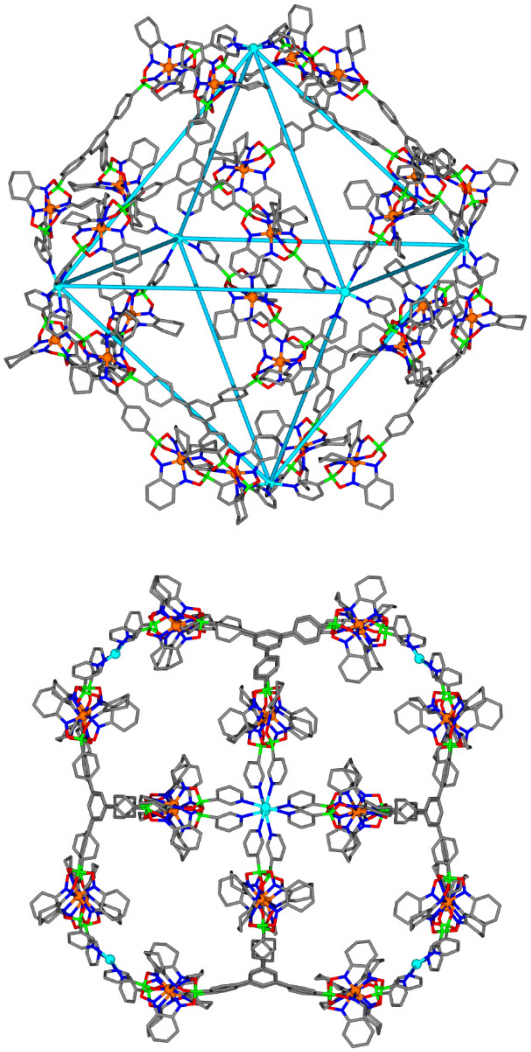

Figure S26. Graphical representation of the structure of cage **2** from the Spartan model. Hydrogen atoms are omitted for clarity. Grey: C; blue: N; green: B; red: O; cyan: Pd and orange:

7. Crystallographic data

Crystals were obtained by the following methods:

- **L1**: Slow diffusion of pentane into a solution of **L1** in DCM.
- **L2**: Slow diffusion of pentane into a solution of **L2** in DCM.
- **1**: Slow diffusion of isopropyl acetate into a solution of **1** in DMSO with the addition of 24 eq. of $NaClO_4$., over the time of several months.
- **2**: Slow diffusion of toluene into a solution of **2** in DMSO or DMSO-*d6*, ., over the time of several months.

Bragg-intensities of **L1**, **L2** and the cage **1** were measured at low temperature using Cu *K*α radiation on a Rigaku SuperNova dual system diffractometer equipped with an Atlas CCD detector for the compounds **L1** and the cage **1** and one equipped with an Atlas S2 CCD detector for the compound **L2**. The datasets were reduced and then corrected for absorption, with the help of a set of faces enclosing the crystals as snugly as possible, with CrysAlis^{Pro}.[S3]

The solutions and refinements for the structures were performed by SHELXT[S4] and SHELXL-2018 (release 3),[S5] respectively. All non-hydrogen atoms were refined anisotropically using full-matrix least-squares based on $|F|^2$. All hydrogen atoms were placed in geometrically calculated positions and refined using a riding model where each H-atom was assigned a fixed isotropic displacement parameter with a value equal to 1.2 U_{eq} of its parent C-atom.

The structure of **L1** was refined as a two-component inversion twin yielding a BASF parameter of 0.48(2). The distance similarity restraint (SADI) was needed for the refinement of the cyclohexyl rings. SIMU and RIGU restraints were also applied on the displacement parameters of the light atoms. Almost, four highly disordered dichloromethane solvent molecules were removed from the model by the SQUEEZE algorithm of PLATON.[S6]

In the case of **L2**, two cyclohexyl moieties and one pyridine ring were disordered over two orientations. The atoms of each orientation were located in a difference Fourier map for each disordered ring. The major and minor parts were refined anisotropically, but distance and similarity restraints (SADI and SIMU) were applied for a convergent least-squares refinement. RIGU restraint was also applied on the displacement parameters of the atoms. Highly disordered solvent molecules were removed with the help of the solvent-masking program in OLEX2.[S7]

The structure of cage **1** was refined as a two-component inversion twin yielding a BASF parameter of 0.50(4). RIGU and SIMU restraints were applied on the displacement parameters of all the atoms and the light atoms, respectively. Aromatic groups were restrained to have an ideal hexagonal geometry, using the card AFIX 66. Some distance similarity restraints (SADI and DFIX) were applied to the cyclohexyl moieties. Additional counter ions and solvent molecules, too disordered to be located in the electron density map, were taken into account using the solvent-masking program in OLEX2.[S7]

Crystallographic data have been deposited to the CCDC and correspond to the following codes: **L1** (CCDC1849686), **L2** (1849685), Cage **1** (1849687). Copies of the data can be obtained free of charge on application to the CCDC, 12 Union Road, Cambridge, CB2 1EZ, U.K. (fax, (internat.) +44-1223-336033; E-mail, deposit@ccdc.cam.ac.uk).

Table S4. Crystal data and structure refinement for **L1**, **L2** and Cage **1**.

Structure identifier	**L1**	**L2**	Cage **1**
Empirical formula	$C_{75}H_{87}B_6Fe_3N_{21}O_{18}$	$C_{93}H_{99}B_6Fe_3N_{21}O_{18}$	$C_{600}H_{696}B_{48}Fe_{24}N_{168}O_{144}Pd_6$
Formula weight (g/mol)	1803.06	2031.34	15062.89
Temperature (K)	140.00(10)	100.00(10)	140.01(10)
Wavelength (Å)	1.54184	1.54184	1.54184
Crystal system	Orthorhombic	Monoclinic	Cubic
Space group	$Pca2_1$	$P2_1/c$	$F432$
a (Å)	35.551(3)	18.0770(18)	52.2358(8)
b (Å)	9.2730(6)	49.704(2)	52.2358(8)
c (Å)	29.6345(18)	12.9398(7)	52.2358(8)
α	90	90	90
β (°)	90	103.811(8)	90
γ	90	90	90
Volume (Å^3)	9769.5(12)	11290.2(14)	142530(7)
Z	4	4	4
Density (calculated) (Mg/m^3)	1.226	1.195	0.702
Absorption coefficient (mm^{-1})	4.101	3.606	2.841
F(000)	3744	4224	31056
Crystal size (mm^3)	0.610 x 0.448 x 0.192	0.277 x 0.070 x 0.014	0.449 x 0.378 x 0.322
θ range for data collection (°)	3.884 to 65.086	2.517 to 74.702	3.688 to 50.429
Index ranges	-41 ≤ h ≤ 41	-21 ≤ h ≤ 22	-52 ≤ h ≤ 52
	-8 ≤ k ≤ 10	-61 ≤ k ≤ 61	-52 ≤ k ≤ 45
	-34 ≤ l ≤ 34	-16 ≤ l ≤ 8	-51 ≤ l ≤ 52
Reflections collected	62177	77535	168420
Independent reflections	16099 [R_{int} = 0.1146]	22430 [R_{int} = 0.1655]	6256 [R_{int} = 0.3215]
Completeness to θ = 65.086°	99.8 %	100.0 %	99.8 %
Absorption correction	Gaussian	Gaussian	Gaussian
Max. and min. transmission	0.715 and 0.128	1.000 and 0.438	0.824 and 0.115
Refinement method	Full-matrix least-squares on F^2	Full-matrix least-squares on F^2	Full-matrix least-squares on F^2
Data / restraints / parameters	16099 / 3070 / 1061	22430 / 1830 / 1339	6256 / 803 / 362
Goodness-of-fit on F^2	1.053	0.890	1.337
Final R indices [I>2σ(I)]	R_1 = 0.1235	R_1 = 0.0871	R_1 = 0.1435
	wR_2 = 0.3170	wR_2 = 0.1704	wR_2 = 0.3646
R indices (all data)	R_1 = 0.1673	R_1 = 0.1799	R_1 = 0.2419
	wR_2 = 0.3566	wR_2 = 0.2296	wR_2 = 0.4521
Largest diff. peak and hole (e.Å^{-3})	2.009 and -0.595	0.623 and -0.412	2.202 and -1.012

Table S5. Determined unit cell dimensions from two differently grown crystals of cage **2**.

	SJ131 - DMSO	SJ125 – DMSO-*d6*
cell_length_a	64.286(8)	64.465(8)
cell_length_b	43.795(3)	43.629(3)
cell_length_c	76.413(7)	76.113(11)
cell_volume	193902(30)	192730(30)
cell_angle_alpha	90.0	90.0
cell_angle_beta	115.668(14)	115.802(16)
cell_angle_gamma	90.0	90.0

8. References

S1 G. Zhang, O. Presly, F. White, I. M. Oppel and M. Mastalerz, *Angew. Chem. Int. Ed.*, 2014, **53**, 1516.

S2 G.J. Kleywegt and T. Jones, *A. Acta Cryst*., 1994, **D50**, 178.

S3 *CrysAlis PRO*. Rigaku Oxford Diffraction 2015.

S4 G. M. Sheldrick, *ActaCryst., Sect. A.*, 2015, **71**, 3.

S5. G. M. Sheldrick, *ActaCryst., Sect. C.*, 2015, **71**, 3.

S6 A. L. Spek, *ActaCryst., Sect C.*, 2015, **C71**, 9.

S7. O. V. Dolomanov, L. J. Bourhis, R. J. Gildea, J. A. K. Howard and H. Puschmann, *J. Appl. Cryst.*, 2009, **42**, 339.